CIRM 10
March 1998

NATIONAL PHYSICAL LABORATORY

Characteristics of multi-energy irradiation fields for determining the near-threshold response of fast-neutron personal dosemeters

by

D.J. Thomas and G.C. Taylor

Centre for Ionising Radiation Metrology

Abstract.
A measurement of the response function for a neutron personal dosemeter normally involves a very extensive series of measurements with accelerator-produced monoenergetic neutrons. These are expensive, and are often impractical for dosimetry services wishing to investigate their dosemeters, particularly if they are attempting to improve the dosemeter response and wish to investigate the effects of various changes in design or processing. A technique is described whereby the variation of the neutron energy with angle for neutron producing reactions such as $^{7}Li(p,n)^{7}Be$ and $T(p,n)^{3}He$ is utilized to irradiate a number of dosemeters to a range of energies in a single experiment. This report describes the characteristics, in particular the angular distribution of the fluence, of three fields covering the energy ranges, 101 to 250 keV, 336 to 565 keV, and 561 to 1200 keV, which between them cover the important energy region where fast-neutron personal dosemeters have a threshold in their detection sensitivity, and where detailed information about the response function is particularly important.
Note: all uncertainties quoted in this report are estimates of standard (1σ) uncertainties representing a confidence level of approximately 67%.

ISSN 1369-6793

National Physical Laboratory
Teddington, Middlesex, UK, TW11 0LW

Approved on behalf of Managing Director NPL, by Dr Julian Hunt
Director, Centre for Ionising Radiation Metrology.

CONTENTS

1. Introduction

1.1 The nature of the problem

In the UK employers are required by law to make estimates of the *effective dose equivalent* received by classified radiation workers. (For definitions of the various dose equivalent quantities used in this document see, for example, ICRU Report 51[1].) In most cases the estimates are obtained by measurements with personal dosemeters. These are designed and calibrated to measure the operational quantity *personal dose equivalent* defined by the International Commission on Radiation Units and Measurements, ICRU. A measurement of this operational quantity is considered acceptable as an estimate of effective dose equivalent in the majority of instances.

For neutron radiation there are, at present, two types of personal dosemeters routinely issued by Approved Dosimetry Services, ADSs, in the UK which are primarily fast-neutron detecting devices. These use either PADC track-etch plastic or NTA film as the sensor element. Albedo dosemeters, for which there is also an ADS in the UK, need a calibration specific to the field in which they are used and these are not considered in this report.

When exposed to neutron bombardment the polymer structure of the plastic poly-allyl diglycol carbonate, PADC, (often known under the trade name CR-39) is damaged by the passage through the material of highly ionising particles, mainly protons produced by neutron scattering. To augment the hydrogen which is in the plastic itself, an additional thin hydrogenous radiator is sometimes included on the surface of the plastic to increase the number of damage sites near the surface. The damage sites are not directly visible, but can be revealed, by chemical or electrochemical etching, which makes them visible as pits when viewed with a microscope. The number of pits per unit area can then be counted, and this number can be related to the neutron fluence or dose equivalent.

In nuclear emulsions, such as NTA film, recoil protons are produced by neutron elastic scattering with hydrogen atoms in the emulsion itself and also in the surrounding hydrogenous material, e.g. the backing, or a radiator element. These recoil protons produce ionisation along their track length and, for any part of the track which is within the emulsion, a latent image is formed as a result of interactions with silver halide grains. After chemical processing, the track becomes visible under a microscope. The shortest identifiable track is about 4 μm in length and consists of three or four developed silver grains, the actual number being dependant on the magnification used. Track densities are usually determined by manually counting the tracks in a given area.

The size of a pit formed in PADC plastic dosemeter, or the length of a track formed in the emulsion of an NTA film dosemeter, depends on the energy of the charged particle producing it, and hence on the neutron energy. As a consequence, both types of dosemeters have an energy threshold below which fast neutrons are not detected because the charged particle recoils do not produce a sufficiently dense ionisation pattern to be registered. This threshold normally occurs in the 100 keV to 200 keV region for PADC plastic, and in the 500 keV to 700 keV region for NTA film.

At the lower end of the neutron energy scale, PADC and NTA dosemeters may respond to thermal neutrons. This can occur either directly or indirectly. NTA film responds directly to thermal neutrons which are captured by nitrogen in the film producing a 600 keV proton which is normally recorded. An example of an indirect response mechanism would be the case where a material containing an element such as boron or nitrogen is included in close proximity to a piece of PADC. Thermal neutrons are captured in the boron or nitrogen with the emission of energetic charged particles which are detected by the plastic. Dosemeters which are sensitive to thermal neutrons also have a sensitivity to epi-thermal neutrons via the thermal albedo from the body of the wearer. There always remains, however, an intermediate energy region where the personal dosemeter's response is negligibly small. As it is possible for a significant proportion of the dose equivalent in a workplace field to occur in that part of this region which is just below the threshold of a PADC or NTA dosemeter, it is important, for estimating the missed dose equivalent, to know exactly where this threshold occurs.

Over recent years numerous workplace neutron spectra have been measured, and others have been calculated. These have recently been collected into a data base of workplace spectra with an associated computer program which allows the response characteristics of neutron sensitive devices in the various spectra to be derived[(2)]. This can be either the fluence response or the dose equivalent response. With this computational tool the potential for under- or over-reading by personal dosemeters can be investigated in real workplace fields. This prediction of the response, however, requires an accurate knowledge of the relevant response function, i.e. the variation of the dosemeter response as a function of energy. This needs to be known over the full energy range where the dosemeter is sensitive. This information is often rather poorly known for PADC and NTA dosemeters, especially in the important region around the energy threshold where the detection efficiency changes rapidly over a small range of neutron energy.

Although it is technically possible to use the NPL Van de Graaff accelerator to investigate the threshold characteristics of personal dosemeters using 'conventional' monoenergetic neutron irradiation techniques, such an approach is time consuming and expensive. This is because each new neutron energy effectively requires the accelerator beam characteristics and the neutron fluence calibration to be re-determined. This involves particle beam alignment (requiring the removal of the neutron-producing target) and fluence measurements using the NPL long counter. The process can easily take an hour or longer.

There is, nevertheless, an increasing level of interest in the implications of the shape of the dosemeter response on recorded doses, and thus a requirement for an improved method of providing response function information over the energy range from 100 keV to 1 MeV.

1.2 A solution to the problem

There are a number of neutron-producing reactions such as $^{7}Li(p,n)^{7}Be$ and $T(p,n)^{3}He$ where the energy of the neutron varies significantly with its angle of emission relative to the direction of the bombarding proton beam. This is a simple consequence of the reaction kinematics, and can be calculated using the laws of momentum and energy conservation. This means that, for physically small devices such as personal dosemeters, it is possible, by arranging them in an arc at different angles relative to the proton beam, to provide simultaneous irradiations of a number of dosemeters at a range of neutron energies. The purpose of the present work was to characterise facilities to provide this type of irradiation on a routine basis.

Unfortunately, there is no single source configuration (i.e. specific reaction and proton energy) capable of producing a variation of neutron energy with angle that covers the whole of the desired energy range. The first part of the work thus involved a study of the available reactions and the reaction kinematics in order to determine how many source configurations would be required to provide an acceptable cover for the energy range of interest with the minimum amount of energy overlap.

As mentioned above, it is possible to calculate the neutron energy at any angle relative to the proton beam from the reaction kinematics. However, the same cannot be said of the fluence rate. Evaluations of the angular distribution of the fluence have been performed[3,4], but the uncertainty in this information is not known and must therefore be assumed to be unacceptably large. Clearly the development of a standard multi-energy neutron irradiation facility requires good knowledge of any inherent uncertainties, and as a consequence it was felt necessary to measure the variation in neutron fluence rate with the angle of emission for the specific target configurations chosen.

The approach of using the variation of energy with angle is not new, and has been used in the past[5]. However, in the absence of any direct experimental measurements, the variation of the fluence with angle relative to the proton beam has had to be taken from published data with large, or even unknown, uncertainties in the fluence delivered at any angle.

1.3 Practical considerations

Personal dosemeter calibrations and response measurements are conventionally performed at NPL at the ISO recommended[6] source to dosemeter distance of 75 cm. The response of fast-neutron personal dosemeters to room scattered neutrons have been shown[7] to be negligible at this distance in the low-scatter neutron irradiation facility associated with the 3.5 MV Van de Graaff accelerator. An existing 'ring' arrangement designed to support personal dosemeters at a fixed distance of 75 cm from a radionuclide source is already available. This provides a suitable arrangement for mounting personal dosemeters in an arc at a fixed distance from the neutron producing target, and for performing dosemeter response function measurements.

Personal dosemeters should be calibrated on-phantom to mimic the backscatter produced by the wearer's body when in normal use. The use of a phantom with the multi-energy facility would not, however, be feasible because of the unacceptable level of general scatter a phantom of the required size would produce, and the irradiations thus have to be performed free-in-air.

In a recent set of measurements, the on-phantom to free-in-air response ratio for PADC and NTA dosemeters has been investigated[8]. The results of this work show that correction factors for the missed backscatter response are small, and can easily be applied. The on-phantom to free-in-air response ratios were determined for ^{241}Am-Be and ^{252}Cf sources. These have, on average, higher energies than required for the multi-energy facility. Backscattered neutrons are of lower energy than those incident on the phantom, and some are thus below the detection threshold of the personal dosemeters. For lower incident energies than those of the ^{241}Am-Be and ^{252}Cf sources, an even greater fraction of the backscattered neutrons will have energies below the threshold. The source based measurements thus provide an upper limit for the correction to be applied for the multi-energy facility. Because the backscatter response is small, only of the order of 5% even for source-emitted neutrons, the uncertainty in the correction for such a small effect will not add significantly to the uncertainty in the response function measurement.

The reading of a single dosemeter has a large statistical uncertainty, usually of the order of 10 to 15%. There is thus a need to irradiate more than one dosemeter at each energy to reduce this uncertainty. The symmetry of the support ring means that corresponding angles on either side of 0° will be subject to the same neutron energy. Most dosemeters are not physically large, and so it is often possible to mount two dosemeters at each position so that four readings are obtained for each energy, with the exception of that corresponding to 0°. For a single energy, four would be a rather small number of dosemeters to irradiate if good statistics are required. However, given that several neutron energies close together are being measured simultaneously, and the fact that the measured response function curve is smooth, a measurement of the final response function with acceptable accuracy can be obtained.

2. The choice of reactions and proton bombarding energies

The selection of source configurations to cover the energy range from roughly 100 keV to 1 MeV was influenced by the existence of an existing multi-energy facility already characterised and used at NPL. This utilises the ^{7}Li(p,n) reaction to cover the energy range from 101 keV to 250 keV. The need was therefore to find additional configurations to cover the region between 250 keV and about 1 MeV.

The range of angles which can be used is restricted to less than 75° on either side of the 0° direction, i.e. the direction of the bombarding proton beam. This is because attenuation of the neutrons in the end plate of the target can assembly becomes increasingly important for angles approaching 90°.

Various bombarding energies were considered in an attempt to cover the greater part of the required energy range with the minimum number of fields. After careful study of the kinematics tables used at NPL to determine neutron energies as a function of angle for a range of charged particle bombarding energies, the most appropriate combinations were found to be:

> the ^{7}Li(p,n) reaction with a proton bombarding energy of 2296 keV producing 565 keV neutrons at 0° with the neutron energy decreasing to 336 keV at 75°; this was designated as Field B, and
>
> the T(p,n) reaction with a proton bombarding energy of 2017 keV producing 1200 keV neutrons at 0° with the neutron energy decreasing to 561 keV at 75°; which was designated as Field C.

The configuration which had already been established, covering the energy range from 101 keV to 250 keV, was designated as Field A. Details of the characteristics of all three fields are given here for completeness.

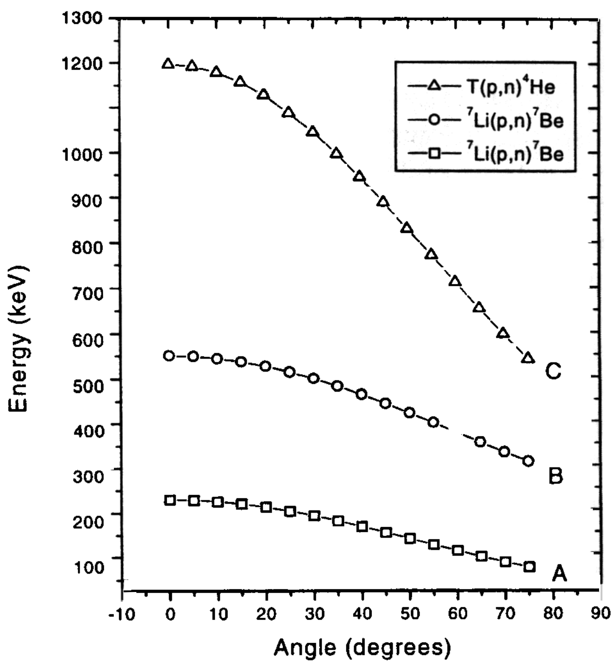

Figure 1. Variation of energy with angle for Fields A, B, and C.

The above combination of fields cover the required energy range reasonably well. The variation of neutron energy with angle is not linear for any of the reactions, as illustrated in Figure 1, and the energy values are closer together for angles near to 0° where the energy is a maximum. This is an unavoidable consequence of the reaction kinematics, but is not a significant problem. At larger angles the energies are more spread out, but even at angles approaching 75°, they are still sufficiently close together if dosemeters are mounted at 5° intervals. The lack of coverage in the neutron energy range 250 keV to 336 keV was not thought to be too important since an interpolation can be performed across this rather small energy gap.

Several considerations influenced the choice of reactions and proton energies. The T(p,n) reaction was also a candidate for Field B. However, the ^{7}Li(p,n) reaction was chosen in preference, firstly because the lithium targets are thinner so that the energy spread of the neutrons, due to slowing down of the proton beam in the neutron-producing target layer, is smaller, and secondly, the neutron fluence rates are higher. The facility based on 565 keV neutron production at 0^0 in fact takes advantage of the maximum in the ^{7}Li(p,n) cross section which occurs at this energy. Neutron yield is thus maximised, which is important in view of the fact that personal dosemeters need to be irradiated to reasonably high dose equivalent levels, of the order of 5 mSv, in order to optimise the number of tracks or pits seen and hence reduce the statistical uncertainty for each dosemeter. The number of tracks or pits should not, however, be too high otherwise overlapping events create problems when reading the dosemeters.

For Field C the obvious reaction is T(p,n) since the ^{7}Li(p,n) reaction does not produce monoenergetic neutrons at energies above 630 keV.

All three fields correspond to neutron energies at 0° which coincide with ISO recommended calibration energies[9]. This has the advantage that the target characteristics, e.g proton energy loss in the neutron-producing layer, for these bombarding energies are already well known from earlier work, as are the approximate 0° neutron yields.

3. Existing information on the angular variation of the fluence

Although kinematic considerations indicate that Fields B and C between them cover the energy range from 336 keV to 1.2 MeV, the fluence rates also need to be reviewed to decide whether the chosen reactions and proton bombarding energies can provide acceptable neutron intensities for irradiating personal dosemeters. From previous fluence determinations for the three 0° energies the approximate maximum fluence and personal dose equivalent rates at 75 cm, i.e. the normal irradiation distance for personal dosemeters, are:

Field A: 250 keV → 1.1×10^3 cm^{-2} s^{-1} corresponding to 0.62 mSv h^{-1},
Field B: 565 keV → 2.8×10^3 cm^{-2} s^{-1} corresponding to 2.6 mSv h^{-1}, and
Field C: 1200 keV → 3.6×10^2 cm^{-2} s^{-1} corresponding to 0.45 mSv h^{-1}.

These figures are only rough estimates of typical values for the targets presently used. By comparison with Field A, the personal dose equivalent rate at 0° is about four times higher for Field B, although for Field C it is about 27% lower. Values for the relative fluence rates are, of course, different, but the personal dose equivalent rates are the most appropriate for comparison since the personal dosemeters are intended to measure this quantity, and should, in principle, have a constant dose equivalent response.

For Field A, the personal dose equivalent at 75°, where the neutron energy is 101 keV, is only 37% of that at 0°. This is much less than would be ideal. A better situation would be at least an equivalent personal dose equivalent rate at 75°. Nevertheless, experiments already performed have shown that it is feasible to make acceptable measurements over the 101 keV to 250 keV range with this field, in the sense that measurable dosemeter readings can be obtained at all energies in a single irradiation, although this irradiation lasts several hours. The variation of fluence with angle for this field is such that the fluence actually initially increases as the angle increases, and over the range from 5° out to 55° is actually larger than at 0°. However, the fluence to dose equivalent conversion factors decrease over this range, because of the decreasing energy.

Nevertheless, the personal dose equivalent rate at 55° is only 66% less than that at 0°. Beyond 55° the decrease in the rate is more rapid.

Estimates of the variation of intensity with angle for Fields B and C can be made, to the accuracy required to ensure that fluence rates are in acceptable ranges, by using the evaluated angular data compiled by Liskien and Paulsen[3, 4]. These estimates are given below.

For Field B, where the 0° energy is 565 keV, the decrease in personal dose equivalent rate with angle is more rapid than for Field A: the value at 55° (420 keV) being 44% of that at 0°, and that at 75° (336 keV) being only 22% of that at 0°. Nevertheless, this was still considered acceptable, mainly because of the higher 0° yield. If the personal dose equivalent values delivered at 0° and 75° in a single irradiation are likely to differ by too large an amount, irradiations can be halted, when the dosemeters around 0° have received an adequate dose equivalent, and these dosemeters removed. The irradiation can then be continued to increase the dose equivalent given to the remaining dosemeters at the larger angles.

For Field C, where the 0° energy is 1200 keV, the 0° personal dose equivalent is lower than for Fields A and B. However, there is some degree of compensation for this in that the yield at larger angles, i.e. greater than about 55°, is a larger fraction of the 0° yield than for the other two cases. The personal dose equivalent at 75° (561 keV) is in fact 41% of that at 0°.

In view of the above considerations, the fluence and dose equivalent rates for the three fields were considered adequate, and an experimental programme was undertaken to measure the angular distribution to the required accuracy.

4. Measurements

Neutrons for the three fields were produced by bombarding neutron-producing targets with protons from the 3.5 MV Van de Graaff accelerator housed in the NPL neutron calibration laboratory. The proton energy was determined by an energy selection magnet whose magnetic field was controlled using an NMR system. This is regularly calibrated using neutron threshold reactions and a p-γ reaction, and proton energies are known to a standard uncertainty of about 1.5 keV. A feedback system, using the current on slits at the exit port where the beam leaves the magnet, is used to feed a signal back to the Van de Graaff energy control system to ensure the proton beam energy remains constant during a measurement.

Two different types of target were used to produce the three fields. For the ^{7}Li(p,n) reactions the target material was approximately 60 μg cm^{-2} of lithium fluoride evaporated onto a 0.25 mm thick silver disk which formed the end plate of the target can assembly. The tritium target consisted of about 19 GBq (0.5 Ci) of tritium absorbed into a layer of about 355 μg cm^{-2} of titanium which had been evaporated onto a 0.25 mm thick gold backing. This in turn was attached to the 0.25 mm thick silver end plate of the target can. (The amount of tritium is somewhat uncertain. The original activity absorbed into the tritium is known, but possible subsequent losses from the layer are hard to quantify.) In both cases the beam passes through the target layer with only a small energy loss, and both target backings were chosen to make neutron production from the backing material negligible. Characteristics of the targets and chosen reactions are summarised in Table 1.

Measurements of the variation in neutron fluence rate with angle for the three fields were performed with the NPL standard long counter[10]. This device has a high neutron detection efficiency, thus allowing measurements at a large number of angles to be performed within a reasonable timescale. The detection efficiency is also roughly constant for neutron energies over the energy range in question.

Table 1. Characteristics of targets and reactions for multi-energy fields.

Field	A	B	C
Neutron energy at 0° (keV)	250	565	1200
Target material	LiF	LiF	Tritium absorbed in a titanium layer
Proton beam energy (keV)	2019	2296	2017
Proton energy loss in the target (keV)	6.2	5.6	40

A long counter consists essentially of a thermal neutron detector, a BF_3 proportional counter tube in the case of the NPL standard long counter, mounted on the axis of a specially designed moderator assembly. Neutron shielding around the sides of the cylinder minimise the sensitivity to neutrons incident on the sides thus giving the device directional detection characteristics. Fast neutrons incident on the end of the cylinder are moderated and a fraction of them are detected in the proportional counter. Signals from this counter are processed using conventional nuclear pulse amplification and shaping techniques. Discrimination between neutron and γ-ray signals in the counter is achieved by setting an appropriate discrimination level, and a logic pulse corresponding to each neutron signal is produced in a pulse shaping unit prior to counting in a scaler system. The shaping unit allows a fixed dead-time to be imposed on each detected event enabling accurate dead-time corrections to be performed.

In addition to neutrons arriving at the long counter directly from the neutron-producing target, other neutrons are detected which arrive at the detector after scattering in the air, or other equipment in the room, or from the floor, walls, or ceiling of the room. Corrections for these scattered neutrons were performed using the *shadow cone technique*. This is a two-stage process which allows the scatter contribution to the reading of the long counter to be measured. The first stage involves selecting an appropriate irradiation distance and angle and then measuring the total fluence rate, i.e. the direct component of interest plus the scattered component. The second stage involves using a *shadow cone* to measure the scattered-only component at the same position. A shadow cone is a neutron shield that is positioned in such a way that it blocks the solid angle from the long counter to the target, stopping the direct neutron component without interfering with the path of the air- and room-scattered neutrons. The direct fluence rate is calculated by subtracting the shadow cone fluence rate from the total fluence rate.

The detector transport system associated with the low-scatter irradiation area of the neutron calibration laboratory is particularly well-suited to the type of measurements needed to characterise the multi-energy field since the stands are mounted on arms which can be moved by remote control to change the angle. Furthermore, because the shadow cone can be mounted on the same arm as the long counter, it is a simple process to perform all the total measurements in one session and then all the scatter measurements in another.

All measurements with the long counter were made relative to monitors which ensured that allowance was made for any variations in the overall output from the neutron producing target. Two monitors were employed, the primary one being the beam current on the target, and the secondary monitor being a moderating device consisting of nineteen BF_3 proportional counter tubes embedded within a block of polyethylene mounted in a fixed position on the wall of the laboratory. The beam current monitor operates by integrating the charge deposited by the beam on the target and producing a pulse for a fixed amount of charge, e.g. one pulse per micro-coulomb. These pulses can be counted in conjunction with counts from the long counter and the wall-mounted monitor.

The path of the proton beam in the evacuated flight line from the Van de Graaff accelerator has been arranged so that the beam does not strike any collimating aperture between the slits at the exit of the energy selection magnet, and the target; a distance of about 20 m. Quadrupole magnets are used to steer and focus the beam to form a 'spot' of about 1 cm diameter at the centre of the disk of neutron-producing target material. This is checked prior to the irradiations by positioning a quartz viewer on the end of the beam line at the position of the target layer. After the beam has been aligned using the quartz, the target is positioned at the end of the beam line, and the controls of the quadrupole magnets are not adjusted in any way thus ensuring that the beam path and beam spot remain unchanged throughout the measurements.

Any loss of target material or movement of the beam spot to an area on the target where the thickness of target material is different would result in a changed output relative to the beam current monitor. To maintain a check that this does not occur the count rate of the wall mounted monitor is constantly checked against the beam current monitor. The count rate of the wall monitor is affected to some small extent by the position of equipment, e.g. the long counter, within the experimental area so that small variations in this ratio, up to about 5%, are to be expected during an experiment. It is for this reason that the beam current is used as the primary monitor. However, the ratio should be the same for a repeat measurement with all equipment in the same position.

Measurements of the angular variation of the fluence were performed in 5° steps extending, in most cases, from at least -80° to at least +80° on either side of 0°. (By convention negative angles are those measured to the left of the beam direction, and positive angles are to the right). Counts were accumulated for total and shadow cone measurements with the long counter until the statistical uncertainty in the derived direct count rate was less than 0.5% for each angle. (Actual values ranged from 0.1% to 0.5%.) The target to long counter distance was set to a value somewhere between 1.5 m and 2.0 m, depending on the field intensity, and was kept constant throughout any one particular measurement. For each field two separate sets of angular data were measured.

5. Analysis

The first step in analysing the data involved dead-time correcting all the measured long counter counts, and then performing a correction for the response to scattered neutrons by subtracting the shadow cone measurement from the total. This provided dead-time corrected values for the count rate per unit current integrator pulse for the direct neutron component from the target.

Uncertainty values were also derived for these data by combining the statistical uncertainty with an additional component covering the small uncertainty in the dead-time correction.

Values for the neutron energy at each angle were then calculated from the kinematics of the reaction, using the known proton bombarding energy, and these neutron energies were used to determine three parameters needed for the remainder of the analysis. The first of these was the efficiency of the long counter at each neutron energy. These values were interpolated from tables of efficiencies as a function of energy maintained for this counter(10). The second parameter was the effective centre of the long counter for each energy. Again these values were obtained from the tabulated data regularly used at NPL. A device like a long counter, which is physically large, in this particular case 46 cm in diameter by 61 cm long, is by no means a point detector, but can act as one for measuring fluence from an essentially point source if allowance is made for the fact that the position of the effective centre lies within the body of the instrument. The third parameter was the air attenuation factor for each energy. Although the shadow cone technique corrects for room scatter into the long counter, it does not allow for neutrons which would have struck the long counter front face, but which were out-scattered by the air between the source of neutrons and the device. A correction for this small effect can be calculated knowing the cross section for attenuation in the air. This can be derived from the individual cross sections for oxygen and nitrogen.

From the long counter data and the above parameters the fluence per current integrator pulse at the position of the effective centre of the counter was first calculated. This was then converted, using the inverse square dependance of the direct fluence, and performing the necessary air attenuation correction, to the fluence per current integrator pulse at 75 cm from the neutron producing target.

The overall yields from the target were not necessarily the same for the two separate measurements of the angular distribution which were made for each field, differences being mainly due to slight variations in the beam 'spot' profile on the target each time the experiment is set up. These differences were never more than about 5%. However, in order to use both sets of data simultaneously to obtain the best parametric fit to the angular distribution, one set of data were always re-normalized to the other by calculating the average difference between values for corresponding angles, and using this average difference as a normalization coefficient. In all cases, after this re-normalization, the two data sets agreed very well.

The best way to describe the shape of the angular distribution, and hence to predict accurately the fluence at any angle from the measured fluence at 0°, is to fit the measured data points to a function which parameterises the distribution shape as well as possible. Angular distributions are normally represented as Legendre polynomials, and since this approach had previously fitted Field A well, the same approach was used for Fields B and C.

The Legendre polynomial expansion provides a means of parameterising the variation of a quantity, y, in this case the neutron yield, with the cosine of the angle θ, in a manner which ensures that the values for y are symmetrical about 0°. The first four terms in the polynomial series, i.e. the expansion up to the third order term, is given by:

$$y = a_0 + a_1\cos\theta + a_2(3\cos^2\theta - \quad)/2 + a_3(5\cos^3\theta - 3\cos\theta)/2 + \qquad \textbf{(1)}$$

where the parameters a_i are the polynomial coefficients which are obtained by fitting the experimental data to the expression.

To perform the fitting, all the data for a particular field were first plotted using the ORIGIN™ scientific graphical package[11]. This has a facility for fitting user defined expressions to data sets using a nonlinear least-squares technique based on the Levenberg-Marquardt algorithm; one of the most widely used algorithms for nonlinear regression. The best fit is found by varying the parameters a_i so that the sum of the squares of the deviations of the theoretical curve from the experimental points is minimised. To perform the fitting a quantity χ^2 is defined by:

$$\chi^2(a_0,a_1, \quad .) = \frac{1}{\quad} \sum_{i=1}^{n} w_i \, [y_i - f(x_i;a_0,a_1, \quad)]^2 \tag{2}$$

where $f(x_i;a_0,a_1,...)$ is the theoretical curve, in this case a Legendre polynomial. The a_i values which minimise χ^2 are found by an iterative process. In Equation (2) n is the number of experimental points, p is the number of adjustable parameters, and the w_i values are the weights. The fitting procedure allows various options such as: the provision of starting values for fitting the parameters a_i, the possibility of fixing some parameters, various types of weighting functions, a choice of the number of iterations, etc.

A number of options were explored when searching for the best fit. Legendre expansions of order 2, 3, and 4 were tried for each field with the criterion of accepting the lowest order which gave a good fit. In addition, both an un-weighted fit and a fit weighted by the inverse square of the standard uncertainty in the fluence at each angle were tried. These uncertainties were derived directly from the uncertainty in the long counter counts, as described earlier, with the addition of a component of 0.3% of the yield to allow for variations in the target-to-long counter distance as the measurement angle changes. (This corresponds to 0.3 cm in a target-to-long counter distance of 200 cm.) No component for the uncertainties in the long counter efficiency or effective centre were included since they would be largely correlated for these data sets. The uncertainty in the efficiency, for example, is estimated to be about 1.5% for a particular neutron energy, but over a small range of energies the uncertainty in the relative efficiencies must be much smaller than this value, and are very difficult to estimate. The same applies for the effective centre.

In all cases the 3rd order polynomial un-weighted fit proved to be the most appropriate and was adopted for all three fields.

The 3rd order fit was always superior to the 2nd order. The 4th order fit tended to result, particularly for Fields A and B, in unrealistic variations in the distribution shape, probably because this order allowed too much freedom to the fitting procedure to try to match features which were in fact a result of statistical variations.

In the case of the weighted fits, when restricted to the range -75° to +75°, the χ^2 values were 1.8, 1.8 and 3.5 for Fields A, B, and C respectively. The fact that this number is slightly greater than the 'ideal' value of 1 probably reflects some missing component in the fluence uncertainties, e.g., that for the uncertainty in the relative efficiencies and effective centres. Nevertheless, the fact that the χ^2 is reasonably close to 1, even without a contribution for the unknown uncertainty components due to the relative efficiencies and effective centres, implies that the fitting function is a satisfactory representation of the shape of the fluence variation with angle.

Because the uncertainties in the fluence were due partly to statistics, the lower fluence values, which occur at the larger angles, had smaller absolute uncertainties than the larger fluences near to 0°. The percentage uncertainties are, of course, smaller for the larger fluences, but the fitting procedure uses absolute uncertainties when calculating weighting factors. Although the differences between the weighted and unweighted fits were very small, there was a slight tendency for the weighted approach to fit the lower fluence values well at the expense of the higher fluence values. Visual inspection of the results indicated that the unweighted fits were marginally more appropriate and these were therefore selected.

A useful measure of the goodness of fit between the experimental data and the fitted curves is the average value of the modulus of the percentage difference between experiment and fit at each angle. For Fields A, B, and C they were 0. 5%, 0.9%, and 0.7% respectively. The indications are thus that the fitted Legendre polynomial expressions allow the fluence at any angle to be predicted from the 0° fluence to an accuracy of 1% or better.

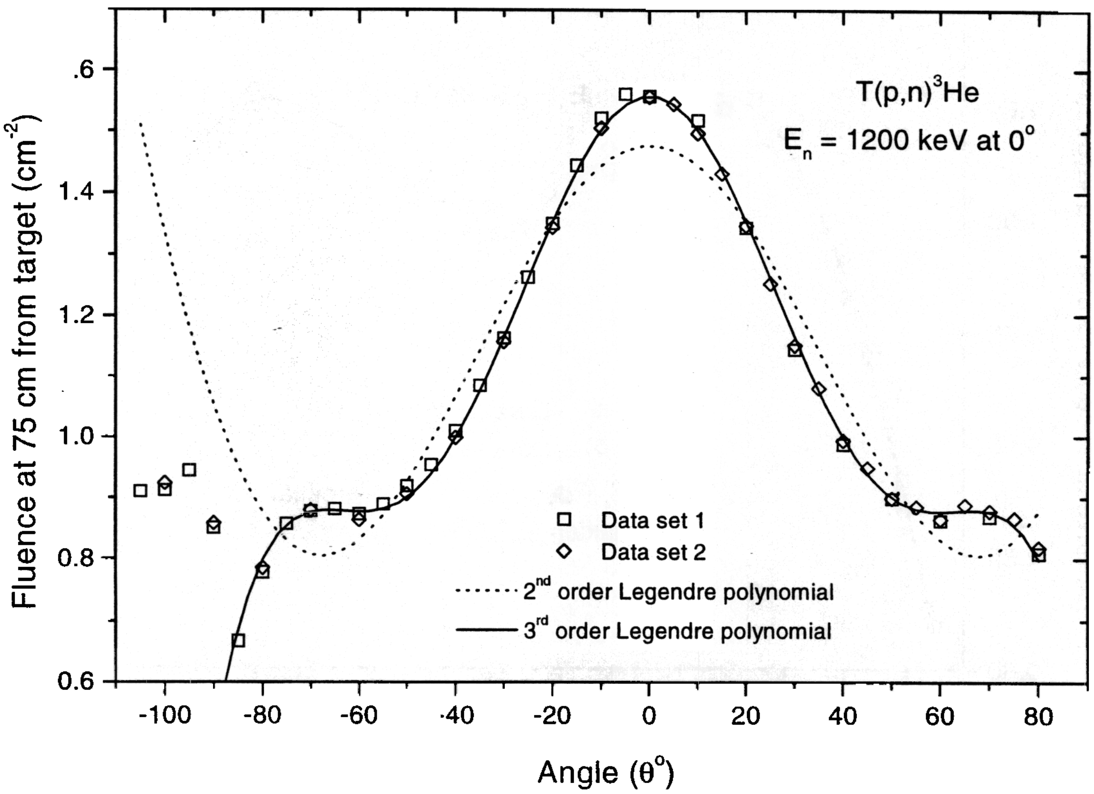

Figure 2. Data for fluence per current integrator pulse at 75 cm from the neutron-producing target for Field C. Also shown are the 2nd and 3rd order Legendre polynomial fits. The error bars representing the uncertainties on the experimental data values are not shown since they are, in all cases, roughly the same size as the symbols.

An example of the experimental data and the fitted curves is presented in Figure 2 which shows the results for Field C. For Fields A and B the differences between the 2nd and 3rd order fits was not large, although the 3rd order fit was somewhat better in both cases. As can be seen from Figure 2, for Field C the 3rd order fit is clearly far superior to the 2nd order fit which is very poor in this case. The measurements for this field were extended to -105°, and show a dip in the region of -85° due to neutron attenuation in the disk at the end of the target can. This dip is more pronounced in this field than in the others for two reasons. Firstly the target can construction is different, with more backing material present. The 0.25 mm gold backing of the tritium target is attached to the end disk of the target can which adds another 0.25 cm layer. For the lithium targets the target backing itself forms the end disk of the target can. Secondly, the decrease in the fluence with increasing angle appears to level off at about 55° for Field C making the dip more apparent.

The reason for fitting the experimental angular distribution data to a mathematical function was to provide a simple means of predicting the fluence at any angle between -75° and + 75° from the fluence measured at 0°. To use the Legendre polynomial expansion for this purpose the fitted coefficients a_i need to be re-normalized so that the 0° fluence calculated using them is unity. The form of the Legendre polynomial dependence on cos (θ) is such that the $y(0°)$ term is equal to the sum of the a_i values. Thus, by dividing each a_i value by the sum of all the a_i values, the distribution is normalized to unit fluence at 0°, and the Legendre expansion with these coefficients provides simple multiplicative factors for deriving the fluence at any angle from that at 0°.

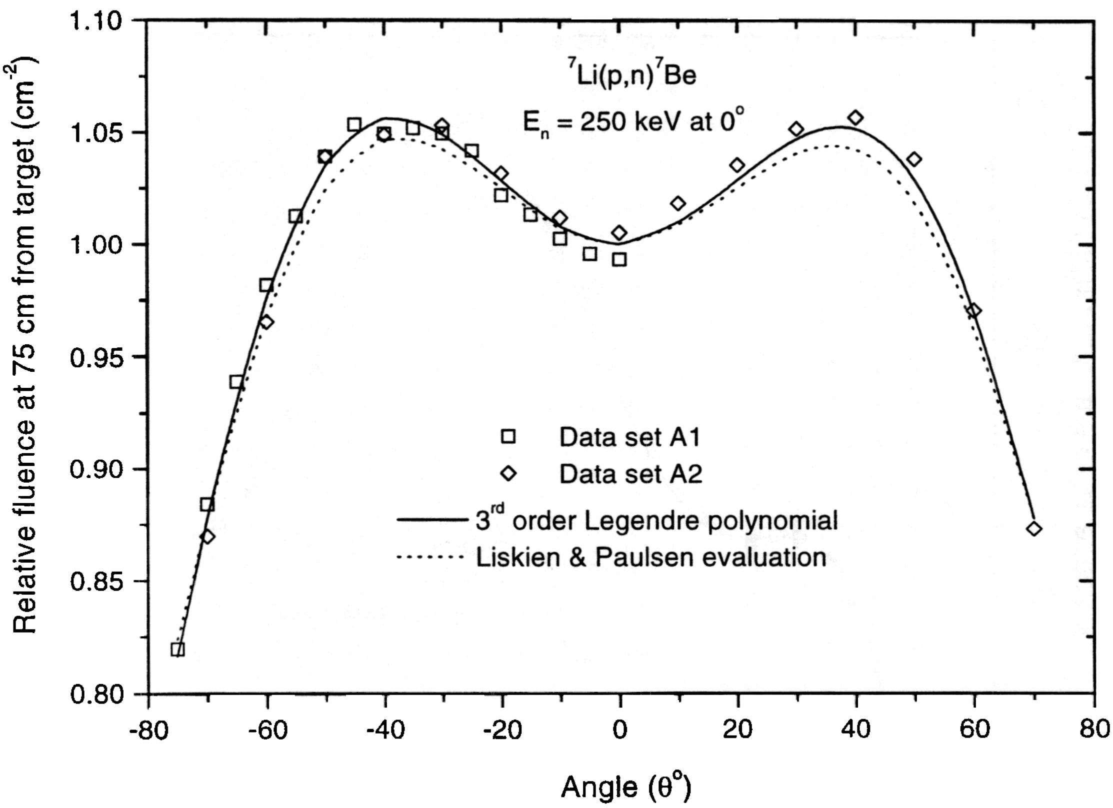

Figure 3. Angular distribution for Field A normalized to unity at 0° showing: the experimental data, the 3rd order Legendre polynomial fit, and the Liskien and Paulsen evaluation. Errors bars for the experimental data are not shown since they are approximately the same size as the symbols.

In Figures 3, 4, and 5 the distributions for Fields A, B, and C respectively are shown with all the data, i.e. both the experimental points and the fitted curves, normalized in this way. The re-normalized a_i values are presented in Table 2.

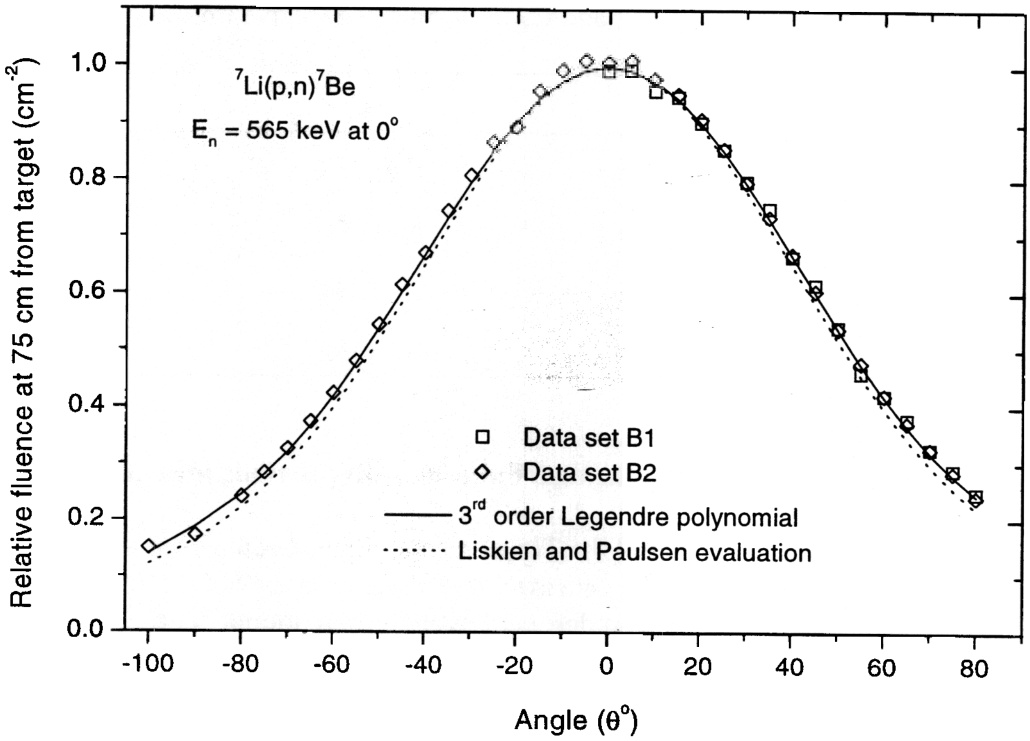

Figure 4. Angular distribution for Field B normalized to unity at 0° showing: the experimental data, the 3rd order Legendre polynomial fit, and the Liskien and Paulsen evaluation. Error bars for the experimental data are not shown since they are generally smaller than the symbols.

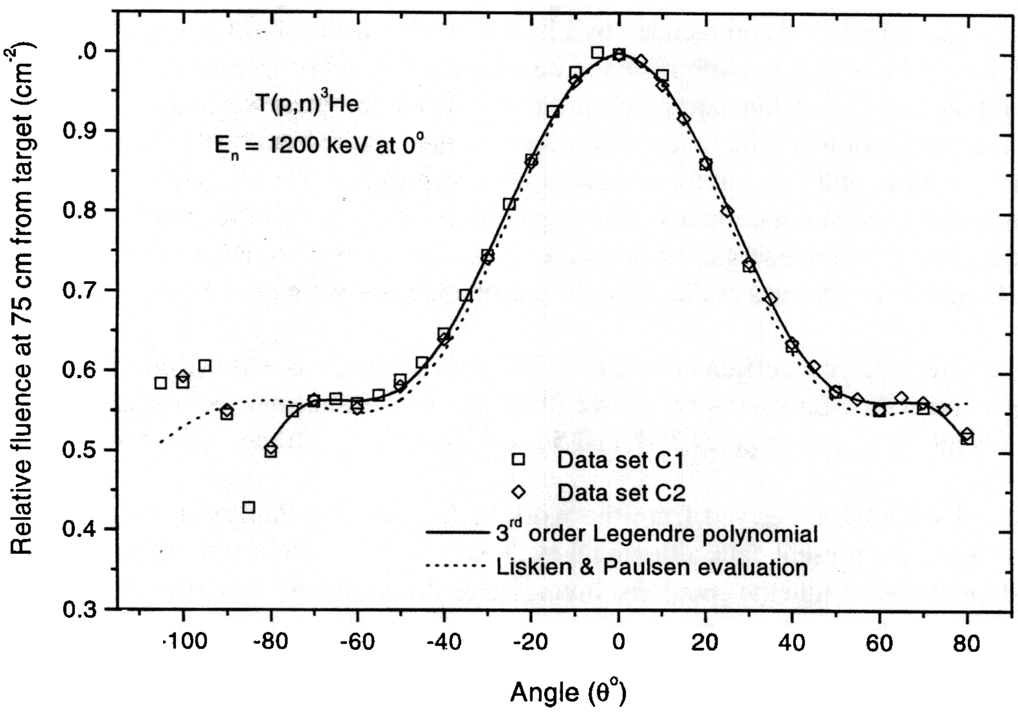

Figure 5. Angular distribution for Field C normalized to unity at 0° showing: the experimental data, the 3rd order polynomial fit, and the Liskien and Paulsen evaluation. Error bars for the experimental data are not shown since they are generally smaller than the symbols.

Table 2. Legendre polynomial coefficients a_i, used to parameterise the laboratory angular distribution for Fields A, B, and C, all normalised to give unit fluence at 0°.

Field	A	B	C
Coefficient a_0	0.62526	0.24578	-0.92158
Coefficient a_1	0.53436	0.49656	3.30809
Coefficient a_2	0.04412	0.11804	-2.48651
Coefficient a_3	-0.20374	0.13962	1.10000

6. Comparison of the present angular distributions with previous measurements

Evaluated data for both the $^7Li(p,n)$ and the T(p,n) reaction have been presented in two reports by Liskien and Paulsen[3, 4]. From all the data available at the time they evaluated the total cross section as a function of energy, and also derived Legendre polynomial coefficients, again as a function of proton bombarding energy, which can be used to predict the differential centre-of-mass cross section at any angle and any energy. Using these parameters tables of the evaluated total and differential cross sections in the laboratory frame were produced for a number of bombarding energies from the neutron threshold to 7 MeV ($^7Li(p,n)$) or 10 MeV (T(p,n)). The differential cross section in the laboratory frame provides a measure of the angular distribution in this frame.

Although the differential cross section data are presented in tabular form for a series of proton bombarding energies, these do not necessarily correspond to the energies used to produce Fields A, B, and C. The approach recommended by Liskien and Paulsen for obtaining data at energies other than those tabulated is to interpolate the Legendre polynomials given in the centre-of-mass system, and to use a Fortran computer program, listed in reference (3), to calculate the differential cross sections in the laboratory system at the required energies. This program was implemented at NPL, and was run for several of the energies tabulated in references (3) and (4) to check that it was working correctly. The Legendre polynomial coefficients in the centre-of-mass system, which for the energies of interest only extend up to 2nd order, were then plotted, as shown on Figure 6, and values at the required proton energies were interpolated graphically.

Using these interpolated coefficients differential cross sections as a function of angle in the laboratory frame were calculated for the three fields and were re-normalised to unit fluence at 0°. These results are plotted in Figures 3, 4, and 5 for comparison with the present work.

The angular distributions derived from the work of Liskien and Paulsen provide reasonable representations of the present data, although they do not fit the experimental points as well as the presently derived fits. While the comparison vindicates the decision to measure the distribution rather than relying on the evaluated data, they also give some reassurance that there were no gross errors in the present measurements. In principle, there should be some differences between the present experimental angular distributions and the evaluated differential cross section. The experimental data are for a particular experimental arrangement, and possibly include some *target scattered* neutrons. Such effects should have been removed from the evaluated data although, in view of the age of the data included in the evaluation (all pre 1975), it is probable that no detailed corrections for target scatter effects had been performed.

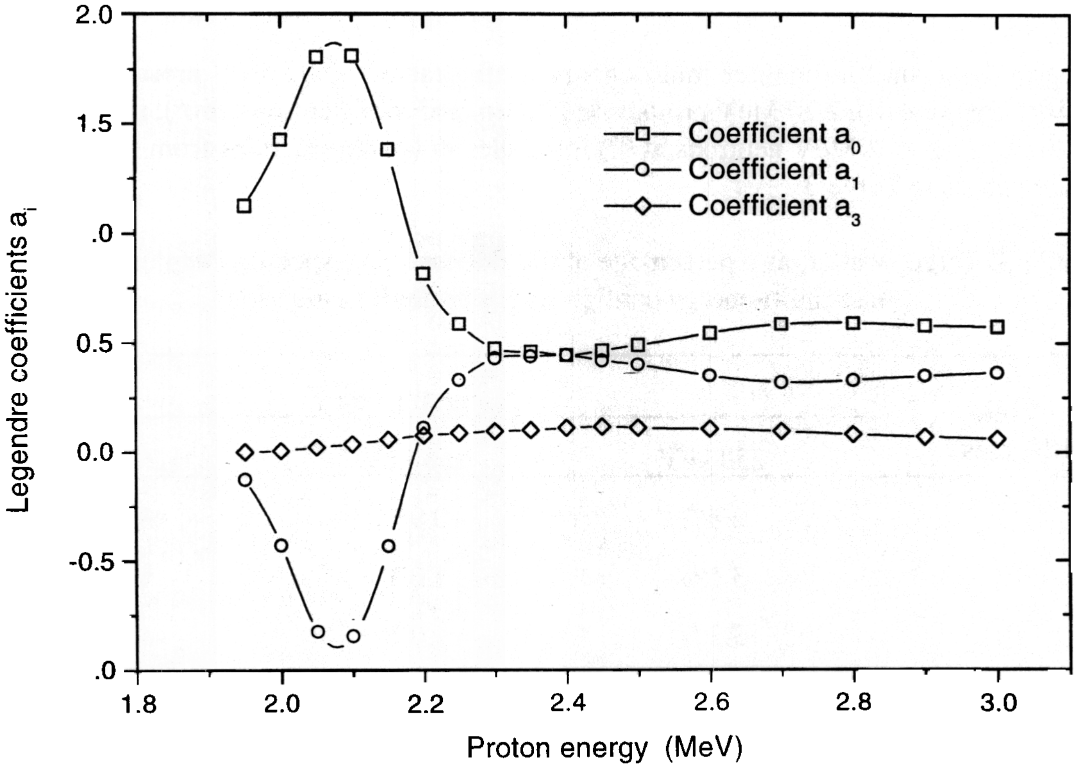

Figure 6. Centre-of-mass Legendre polynomial coefficients for the differential cross section of the $^{7}Li(p,n)^{7}Be$ reaction as evaluated by Liskien and Paulsen(4).

7. Target scattering

The nominally monoenergetic neutrons produced at a particular angle always have an associated distribution of contaminating neutrons, caused by scattering in the target assembly. This is an inherent feature of neutron production using an accelerator and causes problems in interpreting experimental results when the highest accuracy is required. It has, however, been studied in detail(12), both computationally and experimentally, by the German National Standards Laboratory, PTB. The Monte Carlo code TARGET used in these investigations was kindly made available to NPL by PTB to facilitate similar calculations for the NPL target assemblies.

The level of target scattering for the present multi-energy neutron fields has been estimated using the TARGET code, which models simple target assemblies as a series of disks and cylindrical annuli. It tracks each incident charged particle as it slows down through the target layer, allowing for energy and angle straggling, until it undergoes a neutron-producing reaction. The neutron is then tracked through the model, undergoing scattering, absorption, etc., until escaping the model. By specifying a target position and angle, it is possible to calculate how the direct and target-scattered neutron contributions vary with angle.

In addition to the restriction to simple geometries, assembled from the shapes noted above, (although adequate for the present target assemblies), a further limitation is the choice of materials. These are restricted to aluminium, iron, copper, silver, tantalum and water. Consequently, the following approximations had to be made for the present target assemblies:

copper instead of brass for the target can used for the T(p,n) reaction, and iron instead of steel for the target can used for the Li(p,n).

The program was run for the three multi-energy configurations: 2.02 MeV protons on lithium (250 keV neutrons at 0°), 2.30 MeV protons on lithium (565 keV neutrons at 0°), and 2.03 MeV protons on tritium (1.2 MeV neutrons at 0°) for angles in ten degree steps from 0° to 90°. The results are shown in Table 3:

Table 3. Target scatter, as a percentage of the fluence at the specified angles, for the three multi-energy configurations under investigation

Angle (degrees)	Neutron Energy		
	250 keV	565 keV	1.20 MeV
0	2.8%	0.9%	3.5%
10	3.1%	.0%	4.0%
20	3.2%	1.0%	4.5%
30	3.2%	1.2%	5.3%
40	3.2%	1.4%	6.5%
50	3.3%	1.8%	7.2%
60	3.5%	2.2%	7.5%
70	3.9%	3.0%	7.6%
80	4.6%	4.0%	7.7%
90	5.5%	4.8%	7.3%

Independent calculations performed with the Monte Carlo N-Particle transport code MCNP[(13)] for the 2.03 MeV protons on tritium (1.2 MeV neutrons in Table 3) reaction produced the same answer of 3.5% for target scatter, lending confidence to the above results. The MCNP calculations require significant preliminary work to define a 'source term' describing the neutron production in the target layer in terms of both neutron energy and production probability as a function of angle. This has to be compiled from calculations using the reaction kinematics and the neutron production cross section as a function of angle as derived from evaluations[(3, 4)].

Figure 7 shows a comparison between the total neutron spectra predicted by TARGET and MCNP. The agreement is excellent given the two different approaches. The structure observed in the MCNP spectrum, most noticeable between 0.4 and 1.0 MeV, is an artefact of the source definition term's finite angular structure.

One advantage of MCNP is that it can be used to help understand the general structures observed in the spectra by monitoring which parts of the target can assembly the neutrons underwent their last scatter. This is illustrated in Figure 8. The target can consists of a cylindrical tube, 38 mm in diameter and 156 mm long with the target layer deposited, either directly onto the thin circular plate closing one end of the tube, or onto a backing disc which is subsequently attached to the

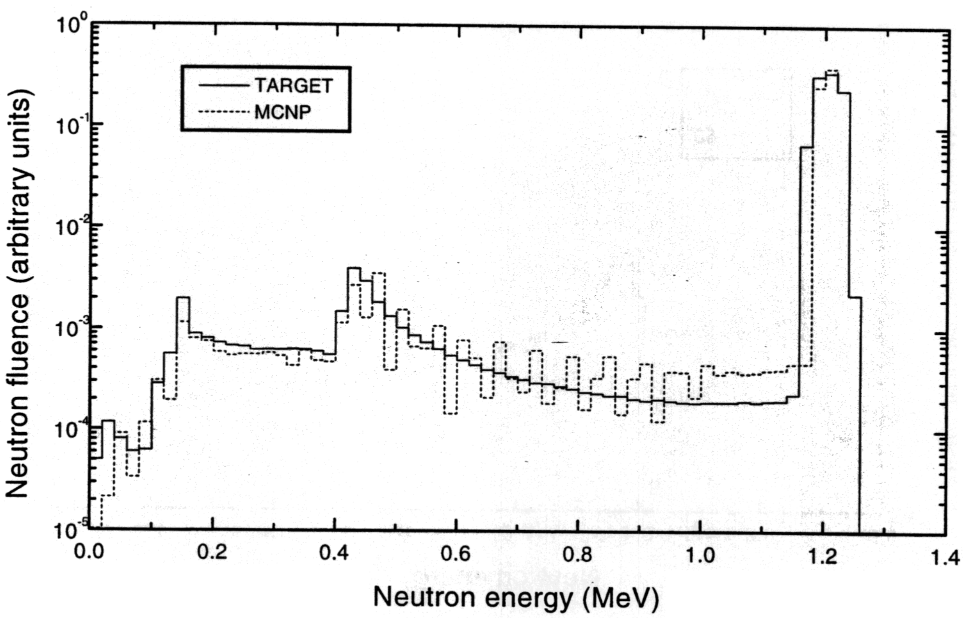

Figure 7. Comparison of target scattering calculations with the TARGET and MCNP codes for the T(p,n)^{3}He reaction producing 1.2 MeV neutrons at 0°.

end plate. The other end of the tube has a flange where the target can is attached to the beam line from the accelerator. From the plot it can clearly be seen that the higher energy scatter comes from the target backing and end plate, with the lower energy scatter coming from the beam tube. Neutrons lose very little energy in a single scatter from the relatively high atomic number

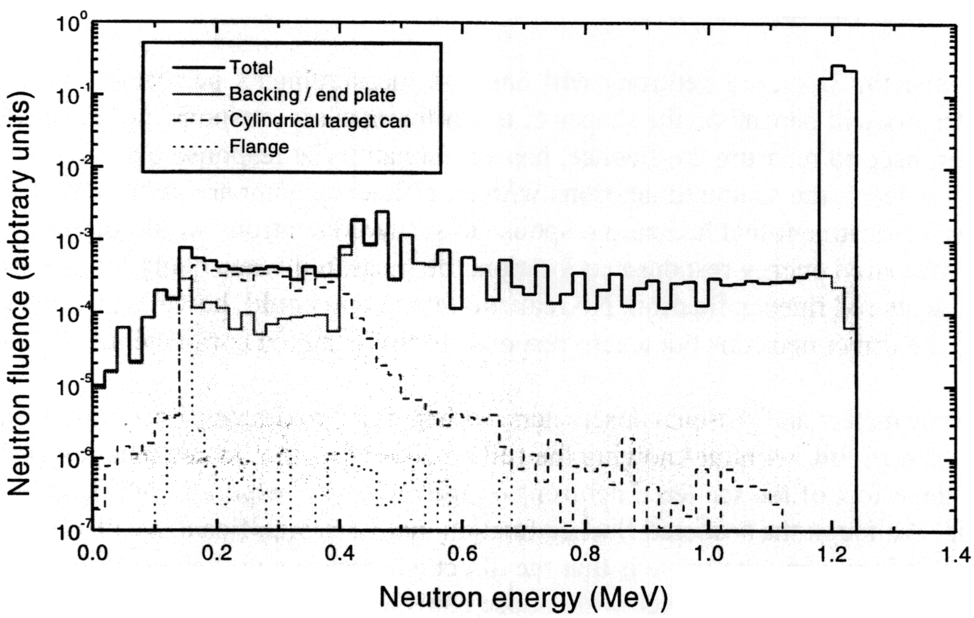

Figure 8. Illustration of where the scattered neutrons underwent their last scatter within the target can for the T(p,n)^{3}He reaction producing 1.2 MeV neutrons at 0°.

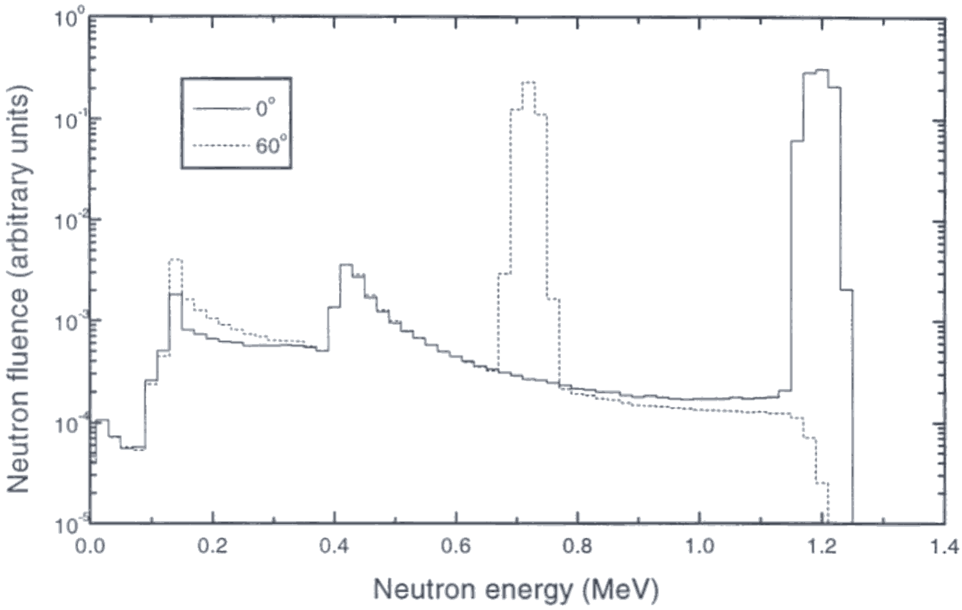

Figure 9. Comparison of spectra, target-scattered plus direct, at two angles relative to the proton beam direction, for the T(p,n)^{3}He reaction producing 1.2 MeV neutrons at 0°.

materials of the target can (a maximum of 8% in a 180° scattering from a material of atomic weight 50) and the energy of a singly scattered neutron simply reflects the angle at which it was emitted from the target.

Although the energy of the direct neutrons falls with increasing angle, this is not the case with the scattered neutrons as demonstrated in Figure 9. This shows that the scattered neutron spectrum at 60° is very similar to that at 0°, even though the direct neutron energy has fallen from 1.2 MeV to about 700 keV.

The effect that the scattered neutrons will have on measurements performed with different neutron detectors will depend on the shapes of the different energy responses of the devices. The long counter, used to measure the fluence, has a reasonably flat response over all energies and will therefore detect the scattered neutrons with an efficiency comparable to that of the direct neutrons. Any instrument that had zero response to scattered neutrons would therefore have an error in its measured energy response calibration, the measured value being low by an amount equal to the scattered fluence fraction. No realistic instrument could, however, have a non-zero response to the direct neutrons but a zero response to the scattered component.

For area survey meters and personal dosemeters, with their approximately dose equivalent energy response, it is difficult, without knowing the full response function in advance, to predict even the sign of the effect of the scattered neutrons on the measured response, particularly at angles other than 0°. Although the scattered fluence fraction increases significantly with angle, another consequence of increasing the angle is that the direct neutrons are no longer the highest-energy component in the spectrum. A device with a dose equivalent response will be more sensitive to those scattered neutrons of higher energy than the direct neutrons, and less sensitive to the neutrons of lower energy. It is therefore possible for an instrument's response calibration to give a result which is either higher, or lower, than the true value as a result of the presence of the scattered component. In no case, for an approximately dose equivalent device, would it, however, be feasible for it to be in error by more than the scatter fraction.

The scattered fluence fraction therefore represents an estimate of the upper limit on the potential error on a response calibration for a roughly dose equivalent device; in reality the actual error will usually be considerably smaller. The actual values are critically dependent on an instrument's energy response and therefore calibration uncertainties will have to be assessed on a case-by-case basis. Potentially problematic instruments are those where the response varies rapidly with energy. For these the response to the scattered component can be radically different to that for the direct component.

8. Conclusions

Fields A, B, and C, whose characteristics and method of production are described in this report, provide an extremely useful facility which will greatly simplify and reduce the cost of measuring fast-neutron personal dosemeter response functions in the energy region around, and just above, the energy where their detection sensitivity exhibits a threshold. This is achieved by utilising the variation of the neutron energy with angle relative to the direction of the bombarding proton beam when using the ^{7}Li(p,n) and T(p,n) reactions. To determine the fluence at any angle, the fluence measured at 0° is multiplied by a factor derived directly from the Legendre polynomial expansion describing the angular distribution of the fluence. Coefficients for the Legendre polynomial expansion are presented here.

The uncertainty in any response characteristic measured with the facility will depend on the uncertainty in the reading of the device. For a personal dosemeter this can be relatively large, typically 10 to 15% for a single dosemeter, and this can often dominate the uncertainty in the measurement. There are various contributions to the uncertainty in the fluence delivered to a device and these are listed below with estimates of typical values.

(a) The uncertainty in the measurement of the neutron fluence at 0° is typically about 4%.

(b) The factors used to derive the fluence at any angle from that at 0° have an uncertainty of about 1% - see Section 5.

(c) Although no correction is made for the effects of room scatter when dosemeters of these types are irradiated at 75 cm from the source of neutrons, an uncertainty component of 1% is included to allow for the uncertainty in the estimate that the response to these scattered neutrons is negligible. Other devices would need to be considered on a case-by-case basis.

(d) For personal dosemeters the absence of a phantom means that there is no phantom backscattered fluence. Corrections can be made for this and uncertainties in the magnitude of the corrections estimated from reference (8).

(e) The uncertainty introduced by target scatter depends on the reaction, the angle, and the device under investigation. Typical vales can be estimated from data in Section 7.

If a calibration is being performed in terms of a dose equivalent quantity rather than neutron fluence, the conversion of fluence to dose equivalent, using recognised conversion coefficients, does not add to the uncertainty since the coefficients are assumed to be exact for monoenergetic energies.

To simplify the analysis of the data three spreadsheets have been set up using the Microsoft Excel application. These are shown in Appendix 1. Each sheet represents one of the Fields A, B or C, and provides a simple means of deriving all the required fluence values, correcting for distance variations, and deriving dose equivalent quantities if required.

Acknowledgements.

This work was funded by the UK National Measurement System Policy Unit and was Deliverable (iv) of Project 3.1 in its 1995 to 1998 Programme for Ionising Radiation Monitoring Metrology. The title of the project was: *An Facility for Determining the Energy Threshold and Near-threshold Response for Neutron Dosimetry.* We would like to thank Dr David Drew for valuable discussions about the facilities, and John Winnington and Andrew Bannett for their efficient operation of the Van de Graaff accelerator.

Appendix 1.

The three following pages show printouts of three rather similar spreadsheets which have been produced to simplify the analysis of experiments using Fields A, B, and C. They represent templates which can be used, either as they stand, or which can be modified if the requirements of a particular experiment demand this. Each sheet provides information about the field being used, and includes options for including routine information about the customer for the irradiations and the date on which it was performed.

Certain data values have to be inserted into the spreadsheet for each irradiation. The first of these is the distance to the dosemeter which has been positioned at 0°. In addition, the vertical offset of the dosemeters above or below the plane of the beam spot must be entered. Ideally this should be zero, but for small dosemeters it is often convenient to irradiate two dosemeters at each angle to increase the number irradiated, in which case one at least of these dosemeters must be displaced from this plane. The spreadsheet uses this displacement distance to calculate the actual angle for the dosemeter. This value is then used in the Legendre polynomial expansion to calculate the factor by which the 0° fluence must be multiplied to give the fluence at the angle of interest. An irradiation with two dosemeters at each angle thus requires two separate sheets for analysis, unless they are displaced by equal distances above and below the horizontal plane of the proton beam. The fluence multiplication factors are displayed as a column on the spreadsheet. The other parameters which need to be entered each time are the actual distances to the dosemeters. When mounted on the irradiation ring the distances, although nominally 75 cm, can vary by a few millimetres.

To derive the fluence at any angle, the fluence at the 0° dosemeter must be entered. This is given as the number of neutrons per cm^2 per currant integrator pulse. The spreadsheets for Fields A and C differ slightly from that of Field B. For Fields A and C the overall number of current integrator pulses recorded during the irradiation is entered on the same line as the value for the fluence per current integrator pulse at 0°. The product of these two numbers then gives the total fluence at 0°. For Field B it is sometimes useful to split the irradiation into two or more time intervals and remove some of the dosemeters positioned around 0°, so that the dosemeters at larger angles are irradiated for longer. In view of the larger variation of fluence and dose equivalent rates with angle for this field, the rates for the larger angles are very much less than for those near 0° and very different total dose equivalent rates are delivered if only a single uninterrupted irradiation is performed. To allow different values for the number of current integrator pulses to be used for different ranges of angles this parameter is included as one of the columns in the spreadsheet.

The energies and the fluence-to-dose equivalent conversion factors, as tabulated in the template spreadsheet shown, may also need to be changed, either because the proton bombarding energy is not set to give exactly the 0° energy shown on the spreadsheet, or if other fluence-to-dose equivalent conversion factors are required.

Multi-energy Field A - Li(p,n) irradiations - 101 to 250 keV energy range

Customer:- **Run No.**

Dosemeter set: *** **Irradiations performed && $$$$$ 199***

Distance at 0 deg for zero offset = 75.0 cm
Dosemeter vertical offset = 0.0 cm

Fluence/CI at 0 deg and 75.0 cm = 6.000E+01 per sq cm per CI CI pulses = 500000

Legendre polynomial coefficients:
a0 = 0.625260
a1 = 0.534360
a2 = 0.044120
a3 = -0.203740

Dose-meter No.	Nominal theta (deg)	Actual theta (deg)	cos(theta)	Energy (keV)	0 deg fluence mult. fact.	Distance (cm)	Fluence at back surface of dosemeter	Conversion factors* (pSv cm2)	Personal dose equiv. mSv
1	-75	-75.00	0.2588	100.9	0.8162	75.0	2.449E+07	70.46	1.725
2	-70	-70.00	0.3420	112.5	0.8778	75.0	2.634E+07	78.27	2.061
3	-65	-65.00	0.4226	124.9	0.9316	75.0	2.795E+07	86.27	2.411
4	-60	-60.00	0.5000	137.9	0.9761	75.0	2.928E+07	94.33	2.762
5	-55	-55.00	0.5736	151.2	1.0106	75.0	3.032E+07	102.47	3.107
6	-50	-50.00	0.6428	164.7	1.0352	75.0	3.106E+07	110.61	3.435
7	-45	-45.00	0.7071	178.1	1.0502	75.0	3.150E+07	118.42	3.731
8	-40	-40.00	0.7660	191.0	1.0565	75.0	3.170E+07	125.73	3.985
9	-35	-35.00	0.8192	203.4	1.0557	75.0	3.167E+07	132.58	4.199
10	-30	-30.00	0.8660	214.9	1.0494	75.0	3.148E+07	138.78	4.369
11	-25	-25.00	0.9063	225.0	1.0397	75.0	3.119E+07	144.09	4.494
12	-20	-20.00	0.9397	233.7	1.0283	75.0	3.085E+07	148.52	4.582
13	-15	-15.00	0.9659	240.8	1.0173	75.0	3.052E+07	152.08	4.641
14	-10	-10.00	0.9848	245.8	1.0081	75.0	3.024E+07	154.69	4.678
15	-5	-5.00	0.9962	249.0	1.0021	75.0	3.006E+07	156.35	4.700
16	0	0.00	1.0000	250.0	1.0000	75.0	3.000E+07	156.87	4.706
17	5	5.00	0.9962	249.0	1.0021	75.0	3.006E+07	156.35	4.700
18	10	10.00	0.9848	245.8	1.0081	75.0	3.024E+07	154.69	4.678
19	15	15.00	0.9659	240.7	1.0173	75.0	3.052E+07	152.08	4.641
20	20	20.00	0.9397	233.7	1.0283	75.0	3.085E+07	148.52	4.582
21	25	25.00	0.9063	225.0	1.0397	75.0	3.119E+07	144.09	4.494
22	30	30.00	0.8660	214.9	1.0494	75.0	3.148E+07	138.78	4.369
23	35	35.00	0.8192	203.4	1.0557	75.0	3.167E+07	132.58	4.199
24	40	40.00	0.7660	191.1	1.0565	75.0	3.170E+07	125.73	3.985
25	45	45.00	0.7071	178.1	1.0502	75.0	3.150E+07	118.42	3.731
26	50	50.00	0.6428	164.7	1.0352	75.0	3.106E+07	110.61	3.435
27	55	55.00	0.5736	151.2	1.0106	75.0	3.032E+07	102.47	3.107
28	60	60.00	0.5000	137.9	0.9761	75.0	2.928E+07	94.33	2.762
29	65	65.00	0.4226	124.9	0.9316	75.0	2.795E+07	86.27	2.411
30	70	70.00	0.3420	112.5	0.8778	75.0	2.634E+07	78.27	2.061
31	75	75.00	0.2588	100.9	0.8162	75.0	2.449E+07	70.46	1.725

* Quantity is Hp(10) AP for an ICRU tissue slab, with ICRP 21 Q(L) relationship, conversion factors from fluence to dose equivalent obtained as a private communication from Hollnagel.

Printed 01-Dec-97

Multi-energy Field B - Li(p,n) irradiations over 336 to 565 keV energy range

Customer:- **Run No.**

Dosemeter set: *** **Irradiations performed && $$$$$$ 199***

Distance at 0 deg for zero offset **75.0 cm**
Dosemeter vertical offset = **0.0 cm**

Fluence/CI at 0 deg and 75.0 cm = **2.000E+02** **per sq cm**

Legendre polynomial coefficients:

a0 =	0.245780
a1 =	0.496560
a2 =	0.118040
a3 =	0.139620

Dose-meter No.	Nominal theta (deg)	Actual theta (deg)	cos(theta)	Energy (keV)	0 deg fluence mult. fact.	Distance (cm)	CI pulses	Fluence at dosemeter	Conv factors* (pSv cm2)	Personal dose equiv mSv
1	-75	-75.00	0.2588	335.9	0.2790	75.0	100000	5.580E+06	203.22	1.134
2	-70	-70.00	0.3420	356.5	0.3196	75.0	100000	6.393E+06	212.64	1.359
3	-65	-65.00	0.4226	377.6	0.3661	75.0	100000	7.322E+06	221.41	1.621
4	-60	-60.00	0.5000	399.0	0.4182	75.0	100000	8.364E+06	229.37	1.919
5	-55	-55.00	0.5736	420.3	0.4756	75.0	100000	9.511E+06	236.29	2.247
6	-50	-50.00	0.6428	441.3	0.5372	75.0	100000	1.074E+07	242.15	2.602
7	-45	-45.00	0.7071	461.7	0.6017	75.0	100000	1.203E+07	246.91	2.971
8	-40	-40.00	0.7660	481.0	0.6675	75.0	100000	1.335E+07	250.58	3.345
9	-35	-35.00	0.8192	499.1	0.7326	75.0	100000	1.465E+07	253.32	3.712
10	-30	-30.00	0.8660	515.5	0.7949	75.0	100000	1.590E+07	255.10	4.056
11	-25	-25.00	0.9063	529.9	0.8523	75.0	100000	1.705E+07	256.26	4.368
12	-20	-20.00	0.9397	542.2	0.9026	75.0	100000	1.805E+07	257.00	4.639
13	-15	-15.00	0.9659	552.0	0.9439	75.0	100000	1.888E+07	257.45	4.860
14	-10	-10.00	0.9848	559.1	0.9746	75.0	100000	1.949E+07	257.72	5.024
15	-5	-5.00	0.9962	563.4	0.9936	75.0	100000	1.987E+07	257.85	5.124
16	0	0.00	1.0000	564.9	1.0000	75.0	100000	2.000E+07	257.90	5.158
17	5	5.00	0.9962	563.4	0.9936	75.0	100000	1.987E+07	257.85	5.124
18	10	10.00	0.9848	559.1	0.9746	75.0	100000	1.949E+07	257.72	5.024
19	15	15.00	0.9659	552.0	0.9439	75.0	100000	1.888E+07	257.45	4.860
20	20	20.00	0.9397	542.2	0.9026	75.0	100000	1.805E+07	257.00	4.639
21	25	25.00	0.9063	529.9	0.8523	75.0	100000	1.705E+07	256.26	4.368
22	30	30.00	0.8660	515.5	0.7949	75.0	100000	1.590E+07	255.10	4.056
23	35	35.00	0.8192	499.1	0.7326	75.0	100000	1.465E+07	253.32	3.712
24	40	40.00	0.7660	481.0	0.6675	75.0	100000	1.335E+07	250.58	3.345
25	45	45.00	0.7071	461.7	0.6017	75.0	100000	1.203E+07	246.91	2.971
26	50	50.00	0.6428	441.3	0.5372	75.0	100000	1.074E+07	242.15	2.602
27	55	55.00	0.5736	420.3	0.4756	75.0	100000	9.511E+06	236.29	2.247
28	60	60.00	0.5000	399.0	0.4182	75.0	100000	8.364E+06	229.37	1.919
29	65	65.00	0.4226	377.6	0.3661	75.0	100000	7.322E+06	221.41	1.621
30	70	70.00	0.3420	356.5	0.3196	75.0	100000	6.393E+06	212.64	1.359
31	75	75.00	0.2588	335.9	0.2790	75.0	100000	5.580E+06	203.22	1.134

* Quantity is Hp(10) AP for an ICRU tissue slab, with ICRP 21 Q(L) relationship; conversion factors from fluence to dose equivalent obtained as a private communication from Hollnagel.

Printed 01-Dec-97

Multi-energy Field C - T(p,n) irradiations for 561 to 1200 keV energy range

Customer:- **Run No.**

Dosemeter set: *** **Irradiations performed && $$$$$$ 199***

Distance at 0 deg for zero offset = 75.0 cm
Dosemeter vertical offset = 0.0 cm

Fluence per CI at 0 deg and 75.0 cm = 1.500E+00 cm-2 per CI pulse 6000000 CI pulses

Legendre polynomial coefficients:
a0 = -0.921580
a1 = 3.308090
a2 = -2.486510
a3 = 1.100000

Dose-meter No.	Nominal theta (deg)	Actual theta (deg)	cos(theta)	Energy (keV)	0 deg fluence mult. fact.	Distance (cm)	Fluence at back surface of dosemeter	Conversion factors* (pSv cm2)	Personal dose equiv. mSv
1	-75	-75.00	0.2588	561.3	0.5487	75.0	4.938E+06	257.79	1.273
2	-70	-70.00	0.3420	613.8	0.5625	75.0	5.062E+06	258.75	1.310
3	-65	-65.00	0.4226	668.8	0.5638	75.0	5.074E+06	260.28	1.321
4	-60	-60.00	0.5000	725.7	0.5620	75.0	5.058E+06	264.67	1.339
5	-55	-55.00	0.5736	783.7	0.5646	75.0	5.081E+06	273.76	1.391
6	-50	-50.00	0.6428	841.7	0.5768	75.0	5.191E+06	288.62	1.498
7	-45	-45.00	0.7071	898.9	0.6015	75.0	5.414E+06	311.52	1.686
8	-40	-40.00	0.7660	954.0	0.6393	75.0	5.754E+06	345.97	1.991
9	-35	-35.00	0.8192	1006.0	0.6888	75.0	6.199E+06	370.64	2.298
10	-30	-30.00	0.8660	1053.8	0.7465	75.0	6.718E+06	367.92	2.472
11	-25	-25.00	0.9063	1096.2	0.8080	75.0	7.272E+06	358.59	2.608
12	-20	-20.00	0.9397	1132.4	0.8682	75.0	7.814E+06	350.63	2.740
13	-15	-15.00	0.9659	1161.5	0.9217	75.0	8.295E+06	348.03	2.887
14	-10	-10.00	0.9848	1182.8	0.9638	75.0	8.675E+06	346.49	3.006
15	-5	-5.00	0.9962	1195.7	0.9907	75.0	8.917E+06	345.69	3.082
16	0	0.00	1.0000	1200.1	1.0000	75.0	9.000E+06	345.44	3.109
17	5	5.00	0.9962	1195.7	0.9907	75.0	8.917E+06	345.69	3.082
18	10	10.00	0.9848	1182.8	0.9638	75.0	8.675E+06	346.49	3.006
19	15	15.00	0.9659	1161.5	0.9217	75.0	8.295E+06	348.03	2.887
20	20	20.00	0.9397	1132.4	0.8682	75.0	7.814E+06	350.63	2.740
21	25	25.00	0.9063	1096.2	0.8080	75.0	7.272E+06	358.59	2.608
22	30	30.00	0.8660	1053.8	0.7465	75.0	6.718E+06	367.92	2.472
23	35	35.00	0.8192	1006.0	0.6888	75.0	6.199E+06	370.64	2.298
24	40	40.00	0.7660	954.0	0.6393	75.0	5.754E+06	345.97	1.991
25	45	45.00	0.7071	898.9	0.6015	75.0	5.414E+06	311.52	1.686
26	50	50.00	0.6428	841.7	0.5768	75.0	5.191E+06	288.62	1.498
27	55	55.00	0.5736	783.7	0.5646	75.0	5.081E+06	273.76	1.391
28	60	60.00	0.5000	725.7	0.5620	75.0	5.058E+06	264.67	1.339
29	65	65.00	0.4226	668.8	0.5638	75.0	5.074E+06	260.28	1.321
30	70	70.00	0.3420	613.8	0.5625	75.0	5.062E+06	258.75	1.310
31	75	75.00	0.2588	561.3	0.5487	75.0	4.938E+06	257.79	1.273

* Quantity is Hp(10) AP for an ICRU tissue slab, with ICRP 21 Q(L) relationship; conversion factors from fluence to dose equivalent obtained as a private communiaction from Hollnagel.

Printed 1-Dec-97

References

(1) International Commission on Radiation Units and Measurements. *Quantities and Units in Radiation Protection Dosimetry,* ICRU Report 51 (ICRU, Bethesda) September 1993.

(2) Naismith, O.F. and Siebert, B.R.L., Manual *for SPKTBIB: a PC-based Catalogue of Neutron Spectra,* NPL Report CIRA(EXT)005, February 1996.

(3) Liskien H. and Paulsen A., *Neutron Production Cross Sections and Energies for the Reactions $T(p,n)^3He$, $D(d,n)^3He$, and $T(d,n)^4He$,* Atomic and Nuclear Data Tables **11**, 569-619, 1973.

(4) Liskien H. and Paulsen A., *Neutron Production Cross Sections and Energies for the Reactions $^7Li(p,n)^7Be$ and $^7Li(p,n)^7Be^*$,* Atomic and Nuclear Data Tables **15**, 57-84, 1975.

(5) Schwartz, R.B. and Hunt, J.B., *Measurement of the Energy Response of Superheated Drop Neutron Detectors,* Radiat. Prot. Dosim. **34,** 377-380, 1990.

(6) International Organization for Standardization, *Procedures for calibrating and determining the response of neutron measuring devices used for radiation protection,* International Standard ISO 10647, 1996.

(7) Taylor, G.C. and Thomas, D.J., *Neutron Scatter Characteristics of the Low-Scatter Facility of the Chadwick Building, NPL,* NPL CIRM Report, in preparation, 1998.

(8) Thomas, D.J., Bartlett, D.T., Burke, M., Horwood, N., Tanner, R., and Taylor, G.C., *Response Characteristics of PADC track etch and NTA film Neutron Personal Dosemeters for Backscatter from Standard calibration Phantoms,* NPL Report CIRM 7, October 1997.

(9) International Organization for Standardization, *Neutron Reference Radiations for Calibrating Neutron-Measuring Devices used for Radiation Protection Purposes and for Determining their Response as a function of Neutron energy,* International Standard ISO 8529, 1989.

Hunt, J.B., *The Calibration and use of Long Counters for the Accurate Measurement of Neutron Flux Density,* NPL Report RS 5, April 1976.

ORIGIN™ User's Manual, MICROCAL™ Software, Inc. Version 4.0, 1995

Guldbakke, S. and Schlegel, D., *The Spectral Neutron Fluence Produced by the Interaction of Charged Particles with Solid State Targets (E_n > 1 MeV),* pp 286-289, Proceedings of the 5th International Conference on Applications of Nuclear Techniques "Neutrons in Research and Industry", Crete, Greece, 9-15 June, edited by George Vourvopoulos, SPIE proceedings series, Volume 2867, 1997.

Briesmeister, J.F. Editor, MCNP™ - *A General Monte Carlo N-Particle Transport Code,* Los Alamos Report LA-12625-M, Version 4B Manual, March 1997.